Proton–carbon monoxide collisions from 10 keV to 14 MeV

E. Wells,[1,2] Vidhya Krishnamurthi,[1] K. D. Carnes,[1] Nora G. Johnson,[2] Heather D. Baxter,[2] David Moore,[1] Kristana M. Bloom,[1] B. M. Barnes,[1,†] H. Tawara,[1,3,‡] and I. Ben-Itzhak[1,*]

[1]*J. R. Macdonald Laboratory, Department of Physics, Kansas State University, Manhattan, Kansas 66506, USA*

[2]*Department of Physics, Augustana College, Sioux Falls, South Dakota 57197, USA*

[3]*National Institute for Fusion Sciences, Nagoya 464-01, Japan*

(Received 13 November 2004; published 29 August 2005)

We have measured relative cross sections and fragmentation branching ratios for proton–carbon monoxide collisions over a wide velocity range from 0.63 to 23.7 a.u. (i.e., E_p of 10 keV to 14 MeV) using a coincidence time-of-flight technique. For low projectile velocity, where electron capture by the projectile becomes important, this process is separated from ionization by projectile charge-state analysis. Our measurements of CO^{2+} production resolve differences between previous measurements, but our multiple-ionization cross-section measurements differ significantly from recent measurements by Siegmann *et al.* [Phys. Rev. A **66**, 052701 (2002)]. The observed kinetic-energy release from dissociating channels varies slowly as the incident proton velocity changes, and in general is not compatible with a simple Coulomb explosion picture.

DOI: 10.1103/PhysRevA.72.022726 PACS number(s): 34.50.Gb

I. INTRODUCTION

Carbon monoxide is an important part of the molecular clouds surrounding galaxies [1], cometary atmospheres [2,3], and the atmospheres of Titan [4] and Triton [5]. Excitation or removal of electrons from CO by cosmic rays, solar wind, or secondary particles stimulates a variety of processes that are important in these environments. It is therefore important to know accurate cross sections and fragmentation patterns for modeling purposes [6]. The same information is also necessary for the understanding of CO in various artificial plasma environments [7].

The ionization of CO by light ions (Ref. [8] provides a review) and, more specifically, protons [9–17], has been studied for a number of years. Most of these studies have focused on measurements of the total-ionization cross section, although some of the more recent experiments include separate cross-section measurements of various final channels. With a few exceptions [15–17], the final-state analysis in these experiments is complicated by the fact that ion detection is uncorrelated. In other words, a C^+ ion from the dissociation of CO^{+*} following the removal of one electron is indistinguishable from a C^+ ion from a dissociating CO^{2+} which has had two electrons removed. Similar problems arise for other dissociating channels. This ambiguity can be removed using multihit detection, for which there are now various techniques [18–23]. In addition, most of these cross-section measurements are restricted either to projectile velocities around 1 (atomic units are used throughout, unless otherwise indicated), where electron capture by the projectile is the dominant mechanism, or to higher velocities, where direct target ionization dominates. At intermediate velocities, where the two processes are comparable, separating the two processes requires additional experimental considerations. We are aware of no previous measurement that spans a large range of velocities, has the ability to detect multiple dissociating ions, and separates the electron capture and ionization channels.

A second class of experiments has focused on the understanding of the molecular decay dynamics in CO, where the decay may be induced by a variety of processes, including single photons, [24–26], intense lasers [27–29], electrons [22,30–32], and ions [21,33–43]. Much of this interest is because the branching ratios between different final states and the kinetic-energy release (KER) from dissociating channels can both provide tests of calculated molecular potential-energy curves. In addition, ion-impact fragmentation of molecules is one example of how electronic energy is transferred to nuclei, and therefore bulk matter. By this mechanism or others, it is clear that the energy initially deposited in electrons results in defects in bulk material via the displacement of atoms [44]. Furthermore, even low-energy charged secondary particles are efficient at producing strand breaks in DNA molecules [45]. Understanding the dynamics of basic ion-molecule collisions is therefore necessary if one hopes to skillfully utilize ionizing radiation at a molecular level for therapeutic purposes.

The reactions under study can be viewed as a two-step process. First, the electrons are either captured by the projectile, excited in the target, or ionized into the continuum. Later, the transient molecular ion can either dissociate or remain as a molecular ion. Therefore, we use the following notation for ionization:

$$H^+ + CO \rightarrow H^+ + CO^{q+} + qe^-, \tag{1}$$

and transfer ionization (TI):

*Electronic address: ibi@phys.ksu.edu

†Present address: Department of Physics, University of Wisconsin, Madison, WI 53706, USA.

‡Present address: Max-Planck-Institut für Kernphysik, D-69029 Heidelberg, Germany.

 ©2005 The American Physical Society

$$H^+ + CO \rightarrow H + CO^{q+} + (q-1)e^-, \quad (2)$$

where in both cases the transient molecular ion CO^{q+} may be in its ground state or excited. If this state is a dissociative state the CO^{q+} will dissociate into $C^{i+}+O^{j+}$ as final products of the reaction. The charge states of the fragments span all possible values from 0 to q, where $q=i+j$ for ionization and $i+j-1$ for TI. Since the dissociation is much slower than the time for electronic rearrangement, the charge of the molecular ion is usually divided symmetrically between the fragments [34,35,42]. However, for the heteronuclear CO, a slight preference of C^+ over O^+ was observed [34,35]. In the case of $q \leqslant 2$ this molecular ion can also be detected as a stable or metastable molecular ion. For $q=1$ the reactions above simplify to single capture defined as

$$H^+ + CO \rightarrow H + CO^+ \quad (3)$$

and single ionization

$$H^+ + CO \rightarrow H^+ + CO^+ + e^-, \quad (4)$$

again with possible dissociative and nondissociative branches.

The simplest picture of the KER distributions generated when the transient molecular ion fragments is the Coulomb explosion model (CEM), which assumes that the initial Coulomb potential energy of the molecular ion is transferred into the kinetic energy of the fragments. Initial experiments [46,47] were in reasonable agreement with the CEM, but lacked the energy resolution for a stringent test. A series of subsequent experiments [33,36,38–40,42,48] resulted in data that could not be fully described with a single KER value based on the CEM or with a reflection of a single vibrational state [49]. For example, it has been shown that the structure in the KER distributions of carbon monoxide dissociating into $C^{i+}+O^{j+}$ matches the Coulomb explosion of higher charges, suggesting that some electrons are excited to states which do not effectively screen the nuclear charge [36,39]. More recently, Tarisien and co-workers [43] used a momentum imaging technique to make KER measurements of the fragmentation of CO after impact by 4 keV/u and 11.4 MeV/u O^{7+}. The reported KER resolution for ion pairs measured in coincidence in this experiment was as low as 250 meV. The rich structure in the observed KER spectra clearly indicated that the molecular dynamics involved in the dissociation were much more complex than the CEM would predict.

In this paper we present the results of a systematic study of proton impact on CO as a function of projectile velocity. Our measured velocities span the range of previous measurements [15,16] at low velocities and considerably extend the range to higher velocities [16]. Using a coincident time-of-flight (CTOF) technique coupled with projectile charge-state analysis for proton velocities where electron capture by the projectile was significant, the various reaction channels were separated. Relative cross sections for all channels were obtained and the branching ratios were determined. Our proton-impact measurements are compared to electron- and antiproton-impact measurements, examining the effect of the sign and mass of the projectile charge. In addition, we obtained KER distributions for both ion-neutral and ion-pair channels, albeit with less resolution than the measurement of Tarisien *et al.* [43].

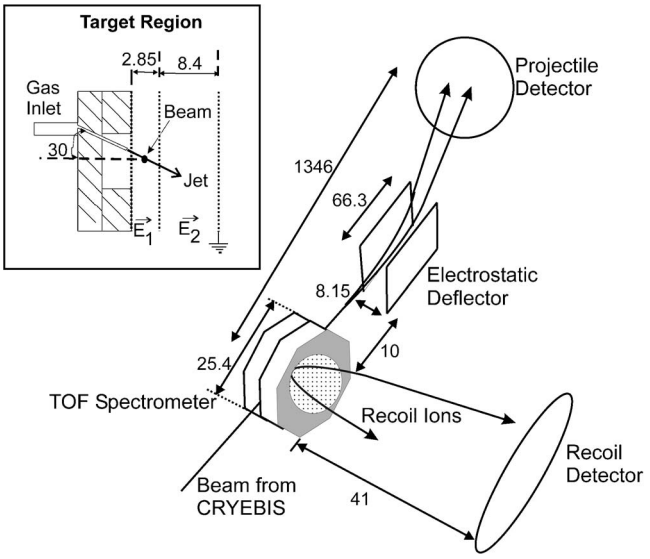

FIG. 1. A schematic view of the low-velocity experimental setup. The inset at the top left shows the target region. Note the angle of the effusive jet. Dimensions on the figure are in millimeters.

II. EXPERIMENT

In order to obtain proton velocities over a wide range, two different accelerators and slightly different experimental setups were used. Each apparatus is described in the following subsections. The data analysis, which was largely the same for both the low- and high-velocity data, is described in the third section.

A. Low-velocity measurements

A beam of protons produced by the KSU-CRYEBIS [50] was accelerated using the source platform voltage, charge separated by an analyzing magnet, and directed toward the target region where it intersected a jet of carbon monoxide. Proton velocities in this part of the experiment ranged from 0.64 to 2.5 a.u. (i.e., $E_p=10$–160 keV). The ion beam was collimated by two sets of slits, separated by about 2 m. An effusive molecular jet localized the target in a strong uniform extraction field (typically about 750 V/cm) which accelerated all recoil ions toward a microchannel plate (MCP) detector, as shown in Fig. 1. The projectiles were charge analyzed after the collision by an electrostatic deflector as well as by the extraction fields on the spectrometer itself. The final charge state of the projectile was determined using a resistive anode two-dimensional position-sensitive MCP detector located about 1.3 m downstream from the target.

The electric fields of the time-of-flight spectrometer must be strong enough to collect all of the energetic molecular-fragment ions produced in the experiment. Transporting the slow, highly charged projectiles through the spectrometer,

however, presents conflicting requirements since a strong extraction field decelerates, steers, and defocuses the ion beam as it travels through the spectrometer. Furthermore, the spectrometer also deflects the ion beam toward the recoil detector. After capture events, the transverse electric field begins to separate the atomic hydrogen projectiles from the H^+ main beam. Care must be taken that both projectile charge states exit the spectrometer. To reduce the competition between these effects, we made the spectrometer very small and reduced the distance from the collision point to the recoil detector, thereby reducing the size of the extraction field needed. The total distance from the collision region to the detector was 57 mm. The spectrometer exit was also widened slightly relative to the entrance, allowing all relevant charge states to exit the spectrometer. In addition, the 66.3-mm-long electrostatic deflector was positioned approximately 1 cm from the spectrometer exit to give maximum control over the projectile charge-state separation. In this configuration, Ar^{11+} at $v=0.20$ and its resulting charge states were successfully transported through the spectrometer. This is near the lower limit possible with this spectrometer, since the (2.2 mm) deflection of the ion beam with a typical 150 V extraction is nearly equal to the (2.85 mm) gap through which the beam is passing. For the higher-velocity and less highly charged beams used in this experiment, the deflection was smaller.

All of the recoil ions produced in a single collision were identified using a coincidence-time-of-flight technique. The times of flight of the different recoil ions were recorded by a multistart system [19,20] relative to a common stop provided by the projectile detector. Typical one- and two-dimensional time-of-flight spectra are shown in Fig. 2. The spectrometer used was a two-stage Wiley-McLaren type [52], similar to the one we have described previously [19,51], although there were a few minor modifications. The most notable modification was the use of a localized jet target. This was accomplished by the addition of a thin tube which directed the target gas through the "pusher" mesh that defined the edge of the extraction field. The gas jet was angled about 30° away from the spectrometer axis to reduce charge exchange between the slow recoil ions and molecules in the jet (see Fig. 1 inset). In addition, the spectrometer dimensions were slightly adjusted from those reported previously [51]. The extraction and acceleration regions of the Wiley-McLaren design were 2.85 and 8.4 mm, respectively, the field-free region 41 mm, and the acceleration region into the channel plate detector remaining unchanged at 5.6 mm.

Besides the addition of the effusive jet, most modifications from our earlier design were necessitated by the conflicting needs of recoil ion extraction and beam transport, as discussed before. Since the spectrometer was only 25 mm along the beam direction, the gap for the beam and the exit for the recoil ions had to be correspondingly small to prevent fringing fields from being significant. The spectrometer consisted of a stack of specially designed, 0.8-mm-thick, double-sided printed circuit boards (PCBs) with their conductive coating forming equally spaced, very-thin-ring electrodes. The inner diameters get larger on successive layers, making a conical exit for the recoil ions. The PCB nearest the collision point had an inner diameter of 4 mm while the one nearest the recoil ion detector had widened to 18 mm. A resistor

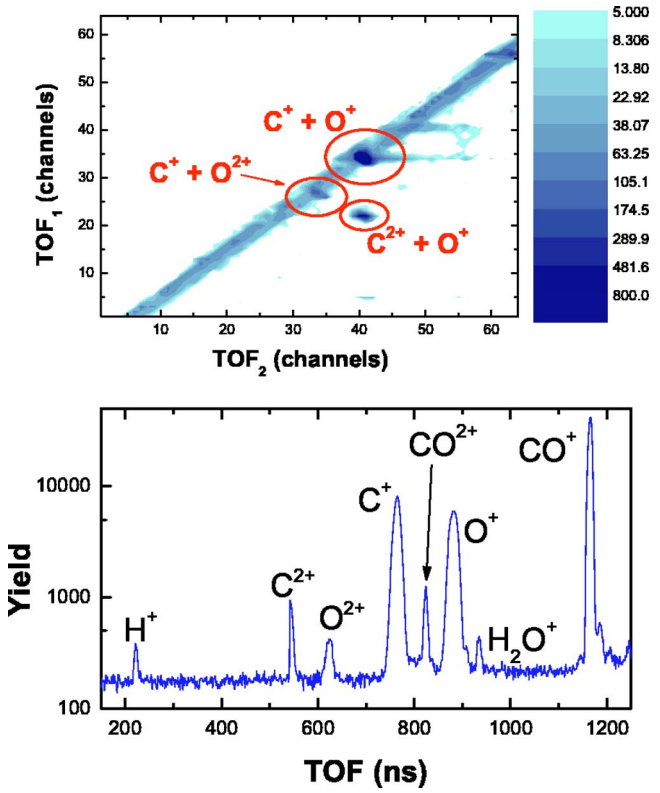

FIG. 2. (Color online) Raw data for the 0.050 MeV H^++CO collision system. Ion-pair events are plotted as a covariance time map on the top and single-ion events are shown as a time-of-flight spectrum in the bottom figure.

chain linked the PCBs so a uniform extraction field was formed. Three 70 line/in. electroform meshes defined the edges of the two-stage Wiley-Mclaren design and the field-free drift region. While the PCBs are not ultrahigh-vacuum compatible, they can be used to create a robust, compact spectrometer. When compressed, the PCB stack is also very flat. Even with the PCB spectrometer, our chamber reached pressures of $\sim 3\times 10^{-7}$ torr, which was sufficient for our experiment. The main drawback of the PCB design was the need to shield all nonconductive areas from stray ions and electrons, resulting in the charging of the spectrometer. An adjustable slit was mounted on the entrance of our spectrometer, which was used to collimate the beam and prevent scattered projectiles (or electrons) from reaching the spectrometer. For the same reason, the spectrometer surfaces on either side of the gap through which the beam is transported were entirely conductive.

The 1.3 m flight length for the projectiles after leaving the target region made for good separation of charge states on the projectile detector (~1 cm), which has a resolution of 0.2 mm. The determination of the projectile charge state was made in off-line analysis of the event-by-event data by first requiring a coincidence with a particular recoil ion to reduce the random projectile yield. The two-dimensional projectile position was then projected onto the axis parallel to the deflector field and fitted with multiple Gaussians to determine the projectile charge-state yield in association with that recoil ion (ions) channel.

B. High-velocity measurements

The apparatus and methods used for the higher-velocity measurements have been described in detail elsewhere [19,20,53] and are only briefly described here. For beam velocities of 6.3–24 a.u. (i.e., E_p=1–14 MeV), a bunched beam of fast protons was accelerated by the tandem Van de Graaff accelerator, collimated, and directed into a target cell containing a thin target of carbon monoxide. The target ions produced were accelerated using a strong extraction field toward a 40-mm-diameter MCP detector. The time-of-flight spectrometer used was a two-stage design similar to the one described in Sec. II A, although it was larger physically. The times of flight of the different ions relative to a signal synchronized with the beam bunch were recorded by two time-to-amplitude converters of a multistop system.

The minimum stable terminal voltage of the Van de Graaff accelerator restricts the production of sub-MeV protons, so for proton velocities of 3.4–6.3 a.u. (i.e., E_p =0.29–1 MeV) a different acceleration method was used. In this technique, described more fully in Ref. [53], OH^- ions are produced from the ion source, accelerated to the terminal, and then dissociated in the gas stripper. This restricts the energy gain for protons in the first stage of the accelerator significantly and allows for measurements in this intermediate-energy range. The beam current, however, is reduced significantly, and when in bunched beam mode there is not enough slit current to provide feedback for accelerator control. Therefore, a dc beam must be used. The TOF of the CO collision products was measured relative to a signal from a projectile detector, consisting of a scintillating detector coupled to a photomultiplier tube (PMT). The detector can run at rates above 1 MHz with a detection efficiency of 1. The PMT signal is passively delayed so it arrives at the timing electronics after the signal from the recoil ion detector. In this arrangement there is some probability that a random projectile, one preceding the proton involved in the collision, may reach the projectile detector before the true projectile. The procedure used to correct these "random stop" events is described in Ref. [53].

C. Data analysis

The data analysis methods used to determine the relative yields in this work are largely the same as what has been described in previous papers [19,35,53], but a few points should be highlighted. First, in our analysis, we have assumed that multiple ionization is isotropic. There is some evidence that this is not the case [17], but we do not expect our data to be significantly affected since in our spectrometer geometry [19], angular discrimination effects are limited to a small part of the target length. The affected length is approximately 10% for the high-energy (tandem) spectrometer, and less for the low-energy (CRYEBIS) spectrometer, which has the advantage of a localized target. Second, we ensure uniform detection efficiency for all ions produced in the collisions by our MCP detector. Moreover, this detection efficiency (ϵ_{det}), which is approximately equal to the product of the open area ratio of the MCP and the transmission of the electroform meshes in the spectrometer, was measured explicitly using fast proton impact on methane (see Ref. [54] for a detailed description of the method). Angular discrimination effects, causing the ion pairs to have a lower extraction efficiency than the molecular ions, thus affecting their overall detection efficiency, were small due to the design of the TOF spectrometer [19]. To improve the accuracy of the reported results the fraction of ion pairs lost due to angular discrimination, η_{ij}, was calculated for each observed ion pair and corrected for, as detailed in [19]. The total ion-pair detection efficiency is then given by $\eta_{ij}\epsilon_{det}^2$. Third, random coincidences and lost fragments were subtracted from the ion-pair and single-ion channels, respectively, [35]. Finally, all measurements were conducted under single-collision conditions, which were tested by a standard pressure dependence.

The kinetic energy released during the dissociation of the molecules can be determined from the time-of-flight information [36,55]. For ion-pair channels, the time difference between arriving fragments is used to determine the KER. This method uses the fact that a narrow range of energies dE_k around the kinetic energy release E_k will produce a flat distribution between the minimum and maximum time differences (see Fig. 2 from Ref. [36]). The width of this distribution depends on the kinetic energy released in the dissociation, while the height depends on the probability for this kinetic energy $P(E_k)$. As developed more fully in Ref. [36], this relationship leads to

$$P(E_k) = [t_{21}(E_k, 0^\circ) - t_{21}(E_k, 180^\circ)] \frac{dt_{21}}{dE_k} \frac{dY}{dt_{21}}, \qquad (5)$$

where $t_{21}(E_k, 0^\circ)$ and $t_{21}(E_k, 180^\circ)$ (i.e., θ=0° and 180° are associated with the short-TOF fragment having initial velocity toward and away from the recoil detector, respectively) are the maximum and minimum time differences, respectively. dY/dt_{21} is the numerical time derivative of the large-time-difference side of the spectrum. For processes in which only one charged fragment is produced, the KER can be determined from the time-of-flight spectra. This technique, as derived by Schäfer *et al.* [55], uses the shape of the time-of-flight spectrum to derive the KER,

$$P(E_k(t)) = \frac{2m}{(qE)^2} \frac{df(t)}{dt}, \qquad (6)$$

where m and q are the fragment mass and charge, respectively, E is the electric field in the extraction region, and $f(t)$ is the number of fragments as a function of their time of flight t. The KER spectra were determined after random-pair and lost-fragment contributions were subtracted as described previously [35,56]. It is important to note that by taking advantage of the event-mode properties of our data collection, these subtractions are done to the time-difference spectra itself, rather than just the total yield of a particular channel.

III. RESULTS AND DISCUSSION

The cross section for nondissociative single ionization of CO by proton impact is shown in Fig. 3. The experimental error is a result of background subtraction, statistics, and normalization. As our data were obtained using three differ-

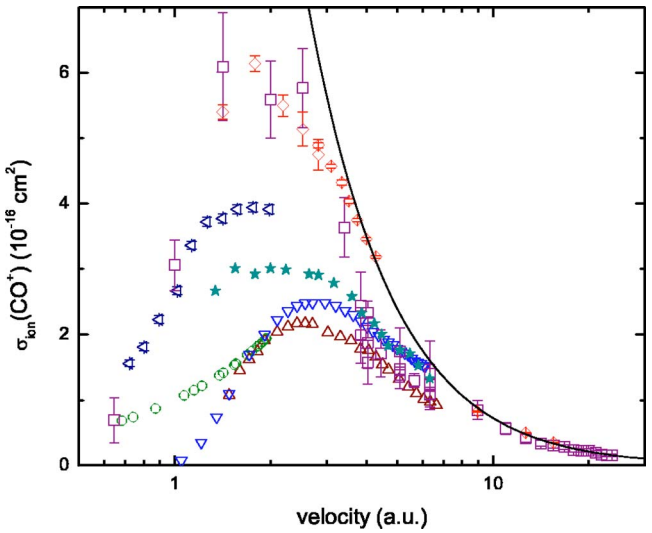

FIG. 3. (Color online) The cross section for nondissociative single ionization of CO as a function of collision velocity for various projectiles. □ represent the present work, ◁ proton impact from Ref. [15], ◇ proton impact from Ref. [16], △ electron impact from Refs. [22,58], ○ electron impact from Ref. [60], ▽ electron impact from Ref. [59], and * the antiproton data from Ref. [16]. The solid line is the semiempirical fit described in Eq. (7) and Ref. [16].

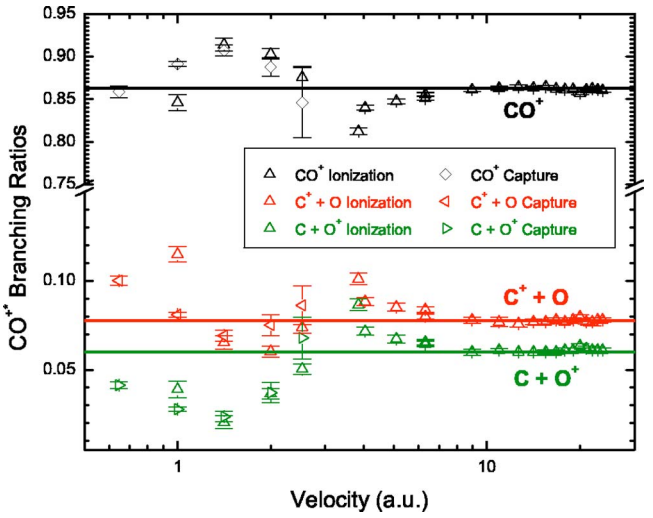

FIG. 4. (Color online) The branching ratio for CO^+ resulting from ionization and capture as a function of projectile velocity. The solid lines represent the average value of the high-velocity data.

ent methods at different proton energies, we normalized each of the three data sets separately. The low-energy measurements [proton energy $(E_p) \leqslant 160$ keV] were normalized to the electron-transfer cross section obtained by Shah and Gilbody at $E_p=26$ keV [15]. The intermediate-energy results (290 keV $\leqslant E_p \leqslant 1$ MeV) were normalized to the single-ionization cross section for 1 MeV H^++He obtained by Shah and Gilbody [15]. Finally, the high-energy data were normalized by measuring the relative single-ionization cross section of CO and He for 4 MeV H^+ impact and then normalizing to the 4 MeV H^++He single-ionization cross section obtained by Knudsen *et al.* [57].

Our data agree reasonably well with the previous measurements for proton impact by Shah and Gilbody [15] and Knudsen *et al.* [16]. At velocities between 1 and 3, our data are in good agreement with the measurements of Knudsen *et al.*, but is 30%–40% above the values reported by Shah and Gilbody [15]. As noted by Knudsen *et al.* [16], the shape of the velocity dependence of the Shah and Gilbody data agrees nicely, so the most likely source of the disagreement is different normalizations. Above 3 a.u. velocity, our measurements are consistently lower than previous measurements, although they merge together nicely toward the high-velocity limit. The high-velocity behavior of the cross section may be modeled semiempirically as described by Knudsen *et al.* in Refs. [16,57]. For CO, the resulting curve is

$$\sigma^+ = \frac{a}{v^2}[1 + b\ \ln(cv^2)] \tag{7}$$

where v is the projectile velocity and constants were determined by Knudsen *et al.* to be $a=50.17$, $b=0.638$, and $c=6.77$ [16].

We have also included in Fig. 3 measurements of ionization of CO by other singly charged projectiles. There are electron data available over the velocity range of interest from Tian and Vidal [22,58], Orient and Srivastava [59], and Mangan, Linsay, and Stebbings [60], as well as antiproton-impact data from Knudsen and co-workers [16]. All of the projectiles merge smoothly into one common curve at high velocity as expected. At lower velocities, however, differences due to the sign and mass of the projectile become apparent. These effects have been discussed in detail elsewhere [16,61,62].

While we have extended the high-velocity range of the cross-section measurement and provided a set of data that extends over nearly the full velocity range of all previous measurements, the distinguishing feature of our measurement is our ability to separate the different final states. Figure 4 shows the branching ratio for removal of one electron from CO. For both electron capture and ionization, the molecular-ion production is the dominant channel. For dissociative final states, production of the lighter C^+ ion is favored over heavier O^+, most likely due to the smaller binding energy for the carbon. The branching ratios show a weak velocity dependence at lower velocities but approach a single value at the high-velocity limit. At this limit, the C^++O channel is about 25% more likely than the C+O^+ channel.

Similar results have been obtained for double, triple, and quadruple ionization at high energy. The results for these charge states of CO are shown in Figs. 5–7. In each case, the branching ratio at high velocities is fairly constant. As has been noted in previous measurements [34,36,42], if ion pairs are produced, the charge is most likely to be divided symmetrically. We observe that if an asymmetric ion pair is produced, electrons are more likely to remain with the oxygen core, leaving the C^{q+} ion more highly charged. For double ionization, shown in Fig. 5, C^++O^+ is the dominant channel, followed by the ion-neutral channel C^{2+}+O and the molecular ion CO^{2+}, with C+O^{2+} the least likely double-ionization channel. In comparison with the electron-impact data of Tian

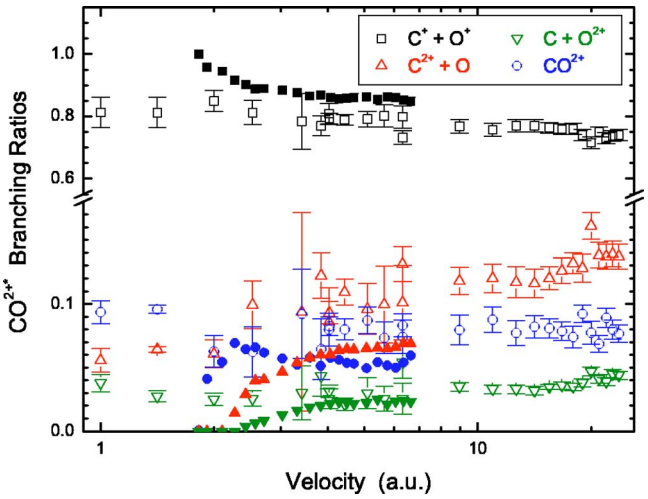

FIG. 5. (Color online) The branching ratio for CO^{2+*} resulting from ionization as a function of projectile velocity. Hollow symbols indicate this work, while the solid symbols are the electron-impact measurements of Tian and Vidal [22]. The uncertainty for the electron-impact data is reported to be 15%.

and Vidal [22], our proton-impact data show about 7–8 % fewer $C^+ + O^+$ ion pairs, and correspondingly more CO^{2+} and $C^{2+} + O$. At low velocities, the $C^+ + O^+$ channel makes up a slightly larger fraction of the branching ratio in both the electron and proton measurements.

For the measured triple-ionization channels, shown in Fig. 6, the branching ratio appears to be almost identical for proton and electron impact. Calculations by Handke *et al.* show some evidence that several excited electronic states of CO^{3+*} might have shallow minima [63–65]; however, we did not observe any CO^{3+} in our measurements. This suggests that the cross section for creating this molecular ion is below $\sim 5 \times 10^{-22}$ cm^2, and/or the CO^{3+} has a lifetime too short to be detected as CO^{3+} in statistically significant levels. C^{2+}

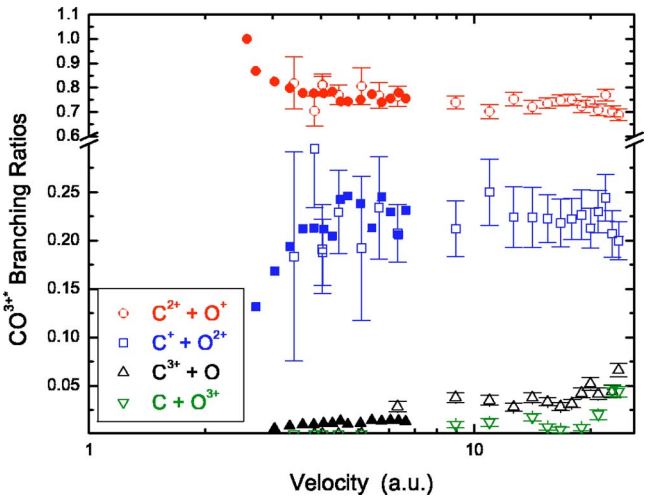

FIG. 6. (Color online) The branching ratio for CO^{3+*} resulting from ionization and capture as a function of projectile velocity. Hollow symbols indicate this work, while the solid symbols are the electron-impact measurements of Tian and Vidal [22,66]. The uncertainty for the electron-impact data is reported to be 15%.

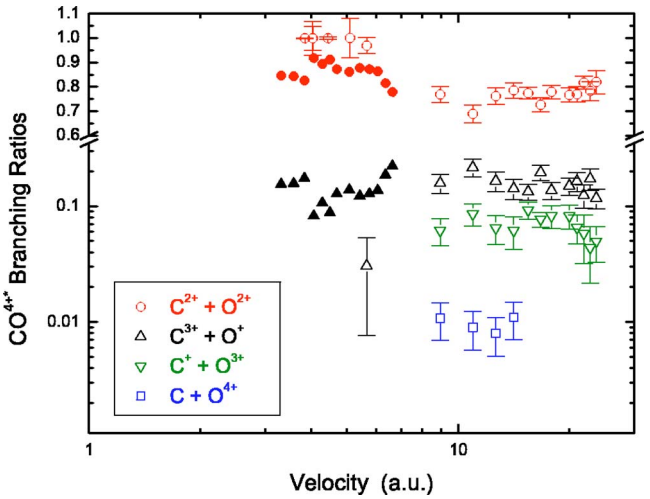

FIG. 7. (Color online) The branching ratio for CO^{4+*} resulting from ionization and capture as a function of projectile velocity. Hollow symbols indicate this work, while the solid symbols are the electron-impact measurements of Tian and Vidal [22]. The uncertainty for the electron-impact data is reported to be 30–40 %. Note that the *y* axis has a logarithmic scale before the break and a linear scale after the break.

$+ O^+$ was about three times as likely as the next most abundant fragmentation channel, $C^+ + O^{2+}$, with the ion-neutral channels significantly smaller, although with a detectable contribution.

The symmetric $C^{2+} + O^{2+}$ channel is the most likely fragmentation channel arising from quadruple ionization of CO, as shown in Fig. 7. The most significant charge-asymmetric channel is $C^{3+} + O^+$. In their electron impact measurements, Tian and Vidal [22] did not observe any other channels associated with four-electron removal. In our data, however, we did observe some $C^+ + O^{3+}$ and, at a few collision energies, a statistically significant value of the ion-neutral channel $C + O^{4+}$. For the channels measured with both proton and electron impact, the branching ratios are similar at the high-velocity end of the proton and electron data. At proton velocities below 6 a.u. our measurements of quadruple ionization show only the main symmetric channel, while the electron-impact data show a significant amount of $C^{3+} + O^+$. A possible explanation is that the PMT technique (see Sec. II B) limits our count rate somewhat, reducing the statistics for a given energy. Our analysis of the main fragmentation channels of CO^{5+*} showed $C^{3+} + O^{2+}$ to be the main channel, followed by the smaller (by a factor of 3–5) $C^{2+} + O^{3+}$ channel.

All of the final channels involving removal, mostly by ionization, of *n* electrons may be summed and compared to the nondissociative single-ionization cross section (shown in Fig. 3) to obtain cross sections for multiple ionization. The cross sections for *n*-fold ionization are shown in Fig. 8. The ionization cross section peaks near a velocity of 2 a.u., dipping as the velocity decreases and electron capture by the projectile becomes the dominant mechanism. The high-velocity tail (i.e., $v > 6$) falls off approximately as $v^{-1.7}$, independent of the number of electrons removed. This results in constant $[(n+1)/n]$-fold ratios for removing an additional

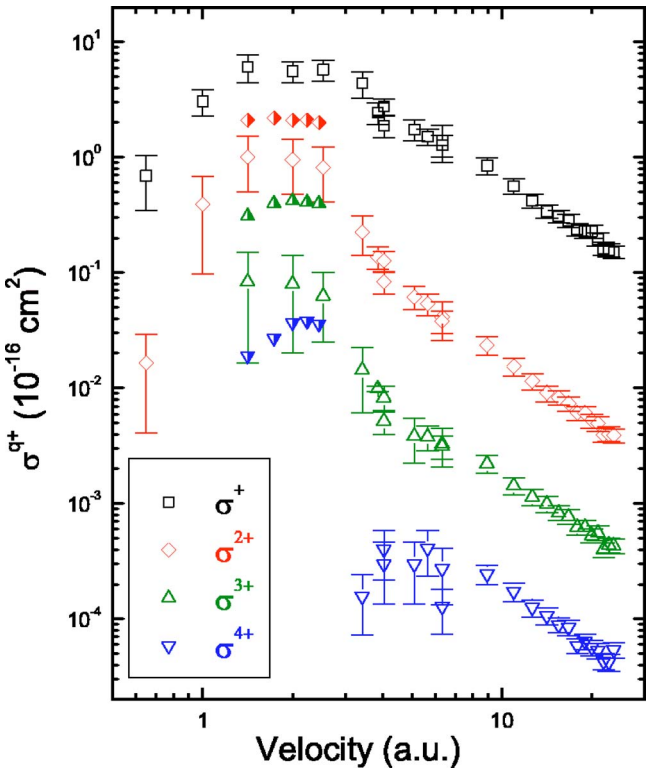

FIG. 8. (Color online) The cross sections for multiple ionization of CO by proton impact as a function of proton velocity. Half-filled symbols are from Siegmann *et al.* [17].

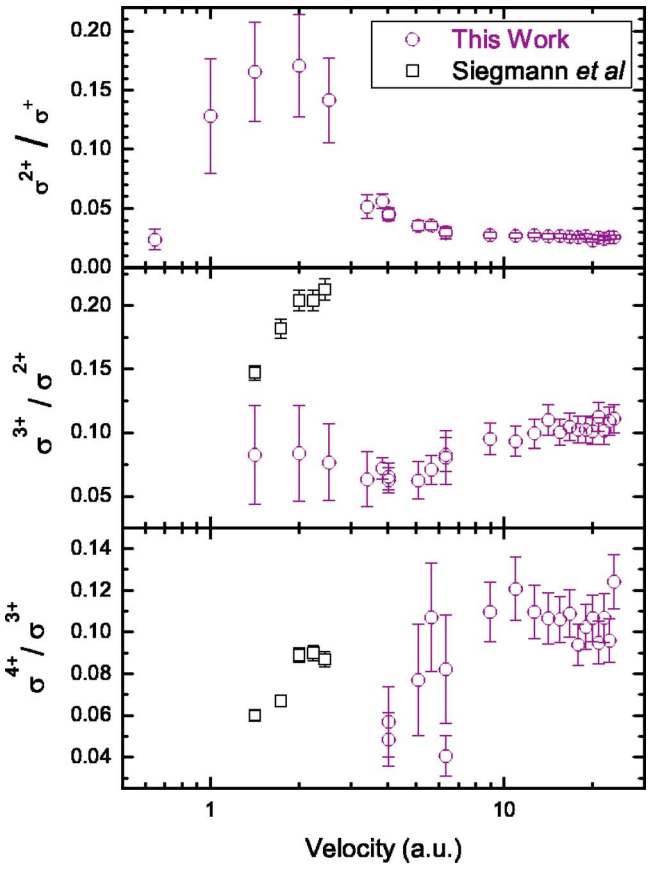

FIG. 9. (Color online) The ratio of multiple-ionization cross sections as a function of proton velocity. The top panel is the double- to single-ionization ratio, the middle panel shows the triple- to double-ionization ratio, and the bottom panel shows the ratio of quadruple to triple ionization. Circles are the present work, while squares are electron-removal data from Ref. [17].

electron, as illustrated in Fig. 9. This is most likely due to the multielectron nature of the target which selects a narrow range of impact parameters for the removal of exactly n electrons within the independent-electron model [67].

In Fig. 8 we also show the two- to four-electron removal cross sections reported recently by Siegmann *et al.* [17]. These cross sections, which were normalized to the theoretical triple-ionization cross section obtained with a statistical energy deposition model [17], are significantly higher than our values. In order to remove the effect of their normalization we show the relative $\sigma^{(n+1)+}/\sigma^{n+}$ cross sections in Fig. 9. Siegmann *et al.* [17] measured a σ^{4+}/σ^{3+} ratio that is higher than our detection limit of quadruple electron removal at low velocities, but it seems to fit the trend of our data. In contrast, their measured σ^{3+}/σ^{2+} ratio is in clear disagreement with our data, both in magnitude and in velocity dependence. The source for this disagreement is not clear, and taking into account that they measured only ion-pair channels while we included also ion-neutral and molecular-ion channels does not resolve the disagreement. However, the disagreement between the relative cross sections is much smaller than the absolute values shown in Fig. 8, thus suggesting that the statistical energy deposition model calculations [17] would not fit our data.

At low velocities ($v \leqslant 2.52$)), separating the projectile charge state allows us to isolate the capture and ionization processes. The measured cross section for single-electron capture is shown in Fig. 10, along with two earlier measurements [15,16]. Our measured values for single-electron capture are in good agreement with the previous data. The relative amounts of capture and ionization in our measurements are shown in Fig. 11 together with the data of Rudd *et al.* [12]. The two data sets exhibit the same velocity dependence, but our data are somewhat higher than the previous

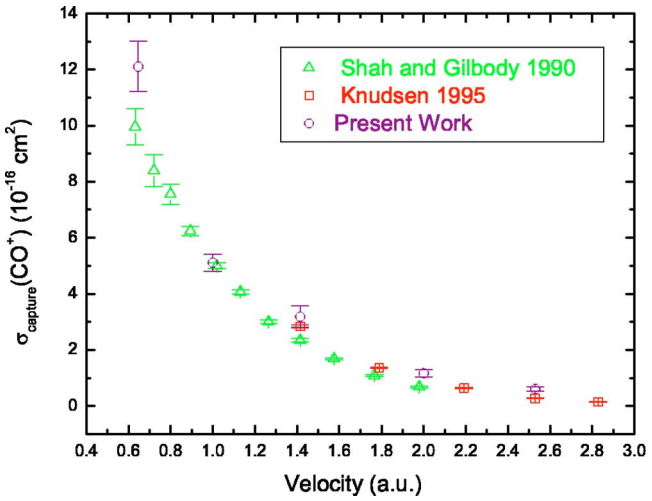

FIG. 10. (Color online) The cross section for electron capture as a function of projectile velocity.

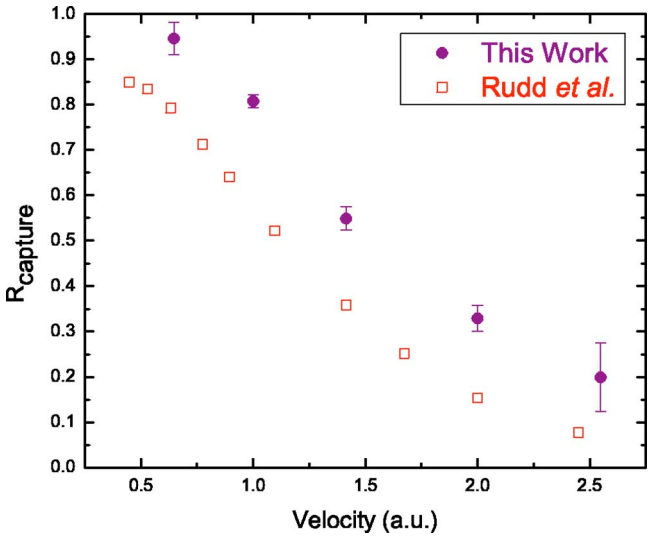

FIG. 11. (Color online) The amount of electron capture relative to all electron-removal processes, $R_{capture}$, as a function of projectile velocity. Our results indicate the relative amount of capture is slightly larger than what was measured in Ref. [12], although the dependence on velocity is very similar.

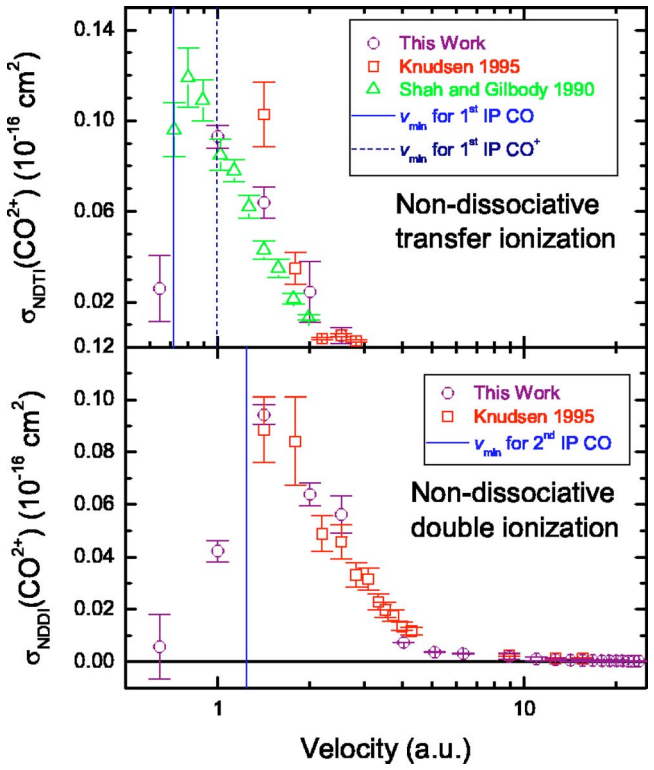

FIG. 12. (Color online) A comparison of CO^{2+} production by different processes.

data. The breakdown of the relative amounts of collision events involving capture and pure ionization are shown for each final molecular channel in Table I. Above $v=2.52$ we did not separate the final charge state of the projectile, so we can make no statements about the relative importance of the capture and ionization channels for those velocities except that extrapolating the trend shown in Fig. 11 suggests that capture becomes relatively smaller with increasing velocity.

As shown in Fig. 5, we observe that long-lived CO^{2+} is a significant part (≈7–8 %) of the two-electron-removal branching ratio. This results from the nature of the CO^{2+} potential-energy curves, as some of the lowest electronic states of CO^{2+} have a deep local minimum and a high barrier limiting dissociation into $C^+ + O^+$. The lower vibrational levels bound in this well result in long-lived metastable states, while higher vibrational levels may decay via tunneling [68–70], or, more likely, predissociation [71–73], on time scales ranging from picoseconds to microseconds. More highly excited electronic states of CO^{2+} are strongly repulsive [25]. The amount of production of this doubly charged molecular ion has been a source of some previous disagree-

TABLE I. The cross sections for various molecular final states in coincidence with H^+ (ionization) and H(*nlm*) (capture) as a function of projectile velocity. The cross sections are given in units of 10^{-19} cm^2. The uncertainty in the absolute cross section is ≈20% for the main CO^+ channel due to normalization. For the other channels, the listed uncertainty represents the statistical error in the measurement relative to the main channel. Note that the uncertainties in the relative cross sections are typically statistical. A dash indicates the signal is below the detection limit.

	v (a.u.)									
	0.64		1		1.41		2		2.52	
Channel	H^+	H(*nlm*)	H^+	H(*nlm*)	H^+	H(*nlm*)	H^+	H(*nlm*)	H^+	H(*nlm*)
CO^+	694	12108	3061	5120	6093	3270	5593	1170	5768	696
CO^{2+}	6±10	26±14	42±4	93±5	94±4	67±7	63±6	24±13	56±4	5±3
$C^+ + O$	77±23	1414±23	416±13	1167±15	436±21	566±21	373±15	232±15	487±14	146±13
$C + O^+$	35±18	584±10	141±14	402±14	137±21	194±21	227±15	115±15	333±16	115±16
$C^{2+} + O$	—	20±10	25±6	80±6	63±6	100±6	61±7	39±7	89±12	35±13
$C + O^{2+}$	—	8±6	17±6	27±9	27±5	35±6	27±6	19±6	23±7	11±6
$C^+ + O^+$	14±4	567±4	365±8	1279±11	797±4	6007±8	853±7	561±7	728±6	347±7
$C^+ + O^{2+}$	—	6±1	6±1	10±1	57±5	80±7	16±2	12±2	19±2	7±3
$C^{2+} + O^+$	—	8±1	16±2	61±5	25±4	390±15	72±1	39±2	53±2	22±4

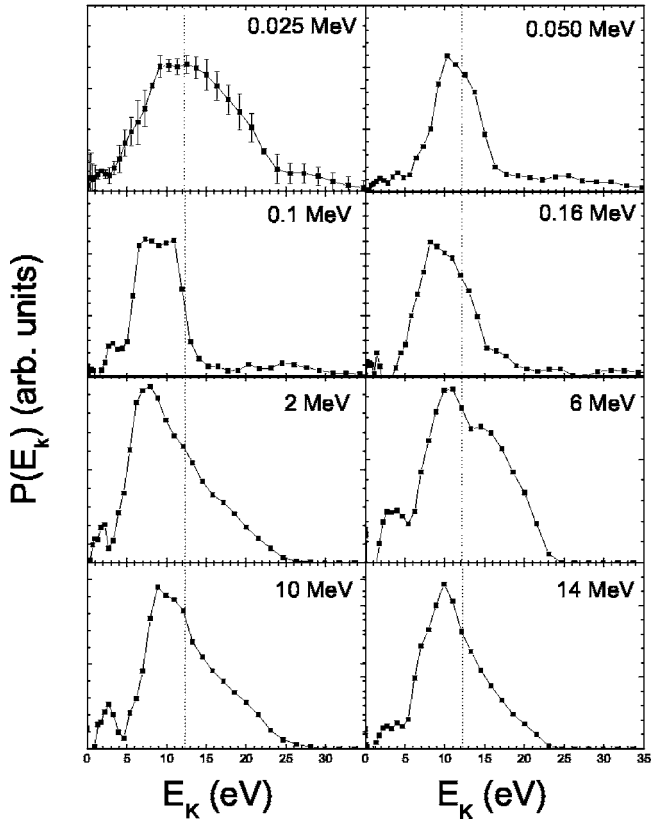

FIG. 13. $P(E_k)$ distributions for $C^+ + O^+$, at a variety of proton energies. The dotted line is the expected peak of the KER distribution predicted from the CEM. The error bars shown on the 0.025 MeV data are of a typical size for all of the KER distributions.

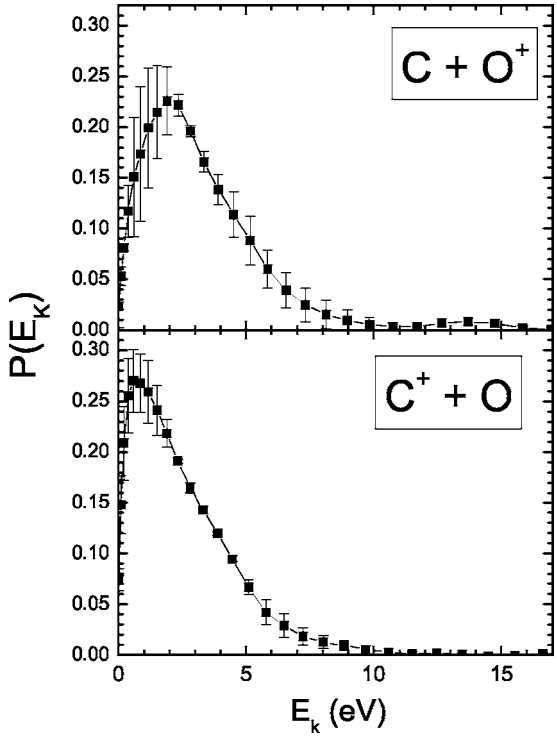

FIG. 14. $P(E_k)$ distributions for $C(nlm)+O^+$ (top) and $C^+ + O(nlm)$ (bottom) final states as a result of 50 keV proton impact. Both capture and ionization processes are included in this figure.

ment in the literature. Shah and Gilbody [10,15] measured significantly less CO^{2+} than in our measurements or the results from Ref. [16]. This difference seems to arise from the inclusion of the nondissociative double-ionization reaction

$$H^+ + CO \rightarrow H^+ + CO^{2+} + 2e^- \tag{8}$$

in our measurements (and those of Knudsen *et al.* [16]) in addition to the nondissociative transfer ionization (NDTI) reaction

$$H^+ + CO \rightarrow H + CO^{2+} + e^-. \tag{9}$$

measured by Shah and Gilbody [15]. As shown in Fig. 12, by separating the pure double ionization in both our data and those of Knudsen *et al.* [16], we find that all three groups are in good agreement for the NDTI cross section, and we are in good agreement with Knudsen *et al.* for the nondissociative double-ionization channel as well.

The CO^{2+} channel is also interesting because the maximum of the cross section for the two different processes shown in Fig. 12 occurs at two different velocities. We interpret this as evidence of threshold behavior in the ionization channel. In a simple picture derived from the Bohr-Lindhard model [74], the threshold for ionization occurs where the release radius is equal to the capture radius. This is satisfied when

$$v_{min} = (z)^{1/4}\sqrt{I_p}, \tag{10}$$

where v_{min} is the threshold projectile velocity, I_p is the ionization potential, and z is the projectile charge. Figure 12 shows v_{min} for the first I_p of CO and CO^+ as well as the second I_p of CO. The onset of NDTI clearly occurs near v_{min} for the first I_p of CO, while the onset of nondissociative double ionization occurs above 1 a.u. velocity, near v_{min} associated with the second I_p of CO. The fact that the NDTI threshold occurs near v_{min} of CO seems to indicate that the ionization step in TI occurs while the captured electron is still close enough to the CO molecule to screen the nuclear charge.

The analysis of the KER distributions for the dissociative channels of CO is summarized in Figs. 13 and 14. In general, the proton-impact data presented here show more structure than the previously reported [36] KER distributions for 19 MeV F^{4+} impact, which were taken with a nearly identical apparatus. The KER distribution of the main ion-pair channel $C^+ + O^+$ shown in Fig. 13 for $v=1$ (i.e., $E_p=25$ keV) peaks very close to 12 eV, which is the KER predicted by the CEM. The distribution, however, is considerably wider than expected from that model or the reflection model, and there is additional unexpected structure at low KER. As the proton velocity increases, the peak of the KER distribution shifts below the value expected from the CEM. At high collision energies ($E_p \geq 1$ MeV), the peak of the KER distribution remains below 12 eV while the high-energy tail of the KER distribution becomes more evident, extending to about 25 eV.

A possible cause of this high-energy tail is dissociation of one state via another due to "curve crossing," which would lead to different KER values. Distinguishing these curve-crossing dissociations requires knowledge of the Q value, and hence the energy of the ejected electrons in the ionization event. A second possibility is that some electrons are left in highly excited states that do not effectively screen the nuclear charge [36,39]. The low-energy component of the distribution most likely results from the dissociation of the CO^{2+*} via predissociation [73]. The gross features of the high- and low-velocity spectra are, however, similar, providing evidence that indicates that the dissociation is governed by the identity of the excited molecular-ion states, rather than the electron-removal mechanism.

In addition to ion-pair channels, we have measured the KER from the dissociation of ion-neutral channels. Some of these states, such as the $C^+ + O(nlm)$ and $C(nlm) + O^+$ channels illustrated in Fig. 14, show significant differences in KER depending on which core retains the vacancy. At $E_p = 50$ keV, the peak of the KER distribution for the $C^+ + O$ channel occurs at just under 1 eV, while the $C + O^+$ channel peaks at nearly three times that value. The small KER in this dissociation is to be expected given the shape of the dissociative CO^+ curves in the Franck-Condon region [75]. Okada and Iwata [75] have calculated potential-energy curves for the $^2\Sigma^+, ^2\Pi, ^2\Delta$, and $^2\Sigma^+$ states of CO^+, which dissociate to either $C^+(^2P) + O(^1D)$ or $C^+(^2P) + O(^2P)$, but not to any $C + O^+$ states. We were unable to locate any calculated potential-energy curves for CO^{+*} states that dissociate to $C + O^+$ in the literature. These high-energy states are not readily comparable to spectroscopic data, so it is perhaps not surprising that structure calculations do not exist. We hope that this result might spur further calculations.

IV. SUMMARY

We have completed a systematic study of proton impact on carbon monoxide over a wide (0.64–24 a.u.) velocity range. Cross sections, branching ratios, and kinetic-energy release distribution measurements have been made for all final states of the transient excited molecular ion. Our branching ratios are remarkably flat over a wide velocity range for all charge states of the transient molecular ion. In general, our results are in good agreement with previous measurements [15,16], although we note a significant incompatibility between our results and the results normalized to the statistical energy deposition model [17]. We have gained an enhanced understanding of CO^{2+} production mechanisms, resolving a long-standing inconsistency in the literature. The gross features of the kinetic-energy release distributions are the same for both capture and ionization, leading us to conclude that both processes result in a roughly similar final-state distribution for the transient molecular ion.

ACKNOWLEDGMENTS

This work was supported by the Chemical Sciences, Geosciences and Biosciences Division, Office of Basic Energy Sciences, Office of Science, U.S. Department of Energy. E.W., N.G.J., and H.D.B. received additional support via the NASA/South Dakota Space Grant Consortium through Cooperative Agreement NGT5-40095 and the Augustana Research/Artist Fund. K.M.B. and B.M.B. were supported by the National Science Foundation's Research Experience for Undergraduates Program.

[1] A. Dalgarno and S. Lepp, in *Atomic, Molecular, and Optical Physics Handbook*, edited by G. F. W. Drake (AIP, Woodbury, NY, 1996).
[2] P. D. Feldman and W. H. Brune, Astrophys. J., Lett. Ed. **209**, L45 (1976).
[3] P. Eberhardt *et al.*, Astron. Astrophys. **187**, 484 (1987).
[4] D. M. Hunten *et al.*, in *Saturn*, edited by F. Vilas, C. R. Chapman, and M. S. Matthews (University of Arizona Press, Tucson, 1988).
[5] V. A. Krasnopolsky, B. R. Sandel, F. Herbert, and R. J. Vervack, J. Geophys. Res. **93**, 3065 (1993).
[6] A. O. Nier, Int. J. Mass Spectrom. Ion Processes **66**, 55 (1985).
[7] *Electron-Impact Ionization*, edited by T. D. Märk, and G. H. Dunn (Springer, New York, 1985).
[8] C. J. Latimer, Adv. At., Mol., Opt. Phys. **30**, 105 (1993).
[9] L. S. Solov'ev, R. N. Il'in, V. A. Oparin, and N. V. Federenko, Sov. Phys. JETP **15** 459 (1962).
[10] R. Browning and H. B. Gilbody, J. Phys. B **1**, 1149 (1968).
[11] V. V. Afrosimov, G. A. Leiko, Yu. A. Mamaev, M. N. Panov, and M. Voiovich, Sov. Phys. JETP **38**, 243 (1974).
[12] M. E. Rudd, R. D. DuBois, L. H. Toburen, C. A. Ratcliffe, and T. V. Goffe, Phys. Rev. A **28** 3244 (1983).
[13] S. L. Varghese, G. Bissinger, J. M. Joyce, and R. Laubert, Phys. Rev. A **31**, 2202 (1985).
[14] F. B. Yousif, B. G. Lindsay, and C. J. Latimer, J. Phys. B **23**, 495 (1990).
[15] M. B. Shah and H. B. Gilbody, J. Phys. B **23**, 1491 (1990).
[16] H. Knudsen, U. Mikkelsen, K. Paludan, K. Kirsebom, S. P. Møller, E. Uggerhøj, J. Slevin, M. Charlton, and E. Morenzoni, J. Phys. B **28**, 3569 (1995).
[17] B. Siegmann, U. Werner, Z. Kaliman, Z. Roller-Lutz, N. M. Kabachnik, and H. O. Lutz, Phys. Rev. A **66**, 052701 (2002).
[18] G. Dujardin, S. Leach, O. Dutuit, P. M. Guyon, and M. Richard-Viard, Chem. Phys. **88**, 339 (1984).
[19] I. Ben-Itzhak, S. G. Ginther, and K. D. Carnes, Nucl. Instrum. Methods Phys. Res. B **66**, 401 (1992).
[20] I. Ben-Itzhak, K. D. Carnes, and B. D. DePaola, Rev. Sci. Instrum. **63**, 5780 (1992).
[21] H. O. Folkerts, F. W. Bliek, M. C. de Jong, R. Hoekstra, and R. Morgenstern, J. Phys. B **30**, 5833 (1997).
[22] Cechan Tian and C. R. Vidal, Phys. Rev. A **59**, 1955 (1999).
[23] J. Ulrich, R. Moshammer, A. Dorn, R. Dörner, L. Ph. H. Schmidt, and H. Schmidt-Böcking, Rep. Prog. Phys. **66**, 1463 (2003).
[24] A. P. Hitchcock, P. Lablanquie, P. Morin, E. Lizon, A. Lugrin,

M. Simon, P. Thiry, and I. Nenner, Phys. Rev. A **37**, 2448 (1988).
[25] P. Lablanquie *et al.*, Phys. Rev. A **40**, 5673 (1989).
[26] A. L. Landers *et al.*, Phys. Rev. Lett. **87**, 013002 (2001).
[27] J. Lavancier, D. Normand, C. Cornaggia, J. Morellec, and H. X. Liu, Phys. Rev. A **43**, 1461 (1991).
[28] K. Codling and L. J. Fansinski, J. Phys. B **26**, 783 (1993).
[29] S. Chelkowski, P. B. Corkum, and A. D. Bandrauk, Phys. Rev. Lett. **82**, 3416 (1999).
[30] K. E. McCulloh and H. M. Rosenstock, J. Chem. Phys. **48**, 2048 (1968).
[31] J. M. Curtis and R. K. Boyd, J. Chem. Phys. **80**, 2035 (1984).
[32] N. Correia, A. Flores-Riveros, and H. Ågren, J. Chem. Phys. **83**, 2035 (1985).
[33] G. Sampoll, R. L. Watson, O. Heber, V. Horvat, K. Wohrer, and M. Chabot, Phys. Rev. A **45**, 2903 (1992).
[34] K. Wohrer, G. Sampoll, R. L. Watson, M. Chabot, O. Heber, and V. Horvat, Phys. Rev. A **46**, 3929 (1992).
[35] I. Ben-Itzhak, S. G. Ginther, and K. D. Carnes, Phys. Rev. A **47**, 2827 (1993).
[36] I. Ben-Itzhak, S. G. Ginther, V. Krishnamurthi, and K. D. Carnes, Phys. Rev. A **51**, 391 (1995).
[37] D. Mathur, E. Krishnakumar, K. Nagesha, V. R. Marathe, V. Krishnamurthi, F. A. Raigara, and U. T. Raheja, J. Phys. B **26**, L141 (1993).
[38] V. Krishnamurthi, I. Ben-Itzhak, and K. D. Carnes, J. Phys. B **29**, 287 (1996).
[39] R. L. Watson, G. Sampoll, V. Horvat, and O. Heber, Phys. Rev. A **53**, 1187 (1996).
[40] H. O. Folkerts, R. Hoekstra, and R. Morgenstern, Phys. Rev. Lett. **77**, 3339 (1996).
[41] H. O. Folkers, T. Schlathölter, R. Hoekstra, and R. Morgenstern, J. Phys. B **30**, 5849 (1997).
[42] L. Adoui, C. Caraby, A. Cassimi, D. Leliévre, J-P Grandin, and A. DuBois, J. Phys. B **32**, 631 (1999).
[43] M. Tarisien, L. Adoui, F. Frémont, D. Lelièvre, L. Guillaume, J-Y Chesnel, H. Zhang, A. Dubois, D. Mather, Sanjay Kumar, M. Krishamurthy, and A. Cassimi, J. Phys. B **33**, L11 (2000).
[44] Chr. Lehmann, in *Defects in Crystalline Solids*, edited by S. Amelinchx, R. Gevers, and J. Nihoul (North-Holland, Amsterdam, 1977), Vol. 10.
[45] B. Doudaïffa, P. Cloutier, D. Hunting, M. A. Huels, and L. Sanche, Science **287**, 1658 (2000).
[46] H. Tawara, T. Tonuma, T. Matsuo, M. Kase, H. Kumagai, and I. Kohno, Nucl. Instrum. Methods Phys. Res. A **262**, 96 (1987).
[47] T. Matsuo, T. Tonuma, M. Kase, T. Kambara, H. Kumogai, and H. Tawara, Chem. Phys. **121**, 93 (1988).
[48] C. Caraby, L. Adoiu, J. P. Gradin, and A. Cassimi, Eur. Phys. J. D **2**, 53 (1998).
[49] H. D. Hagstrum and J. T. Tate, Phys. Rev. **59**, 354 (1941).
[50] M. P. Stöckli, P. E. Gibson, C. L. Cocke, B. D. DePaola, D. Fry, S. Kravis, D. Parks, P. Richard, T. N. Tipping, B. Walch, and S. Winecki, Rev. Sci. Instrum. **67**, 1162 (1996).
[51] I. Ben-Itzhak, E. Wells, M. P. Stöckli, H. Tawara, and K. D. Carnes, Phys. Scr., T **73**, 270 (1997).
[52] W. C. Wiley and I. H. McLaren, Rev. Sci. Instrum. **26**, 2903 (1955).
[53] I. Ben-Itzhak, E. Wells, D. Studanski, V. Krishnamurthi, K. D. Carnes, and H. Knudsen, J. Phys. B **34**, 1143 (2001).
[54] I. Ben-Itzhak, K. D. Carnes, S. G. Ginther, D. T. Johnson, P. J. Norris, and O. L. Weaver, Nucl. Instrum. Methods Phys. Res. B **79**, 138 (1993).
[55] K. Schäfer, W. Y. Baek, K. Förster, D. Gassen, and W. Neuwrith, Z. Phys. D: At., Mol. Clusters **21**, 137 (1991).
[56] A. M. Sayler, J. W. Maseberg, D. Hathiramani, K. D. Carnes, and I. Ben-Itzhak, in *Application of Accelerators in Research and Industry*, edited by J. L. Duggan and I. L. Morgan (AIP, Melville, NY, 2003), p. 48.
[57] H. Knudsen, L. H. Andersen, P. Hvelplund, G. Astner, H. Cederquist, H. Danared, L. Liljeby, and K-G Rensfelt, J. Phys. B **17**, 3545 (1984).
[58] Cechan Tian and C. R. Vidal, J. Phys. B **31**, 895 (1998).
[59] O. J. Orient and S. K. Srivastava, J. Phys. B **20**, 3923 (1987).
[60] M. A. Mangan, B. G. Lindsay, and R. F. Stebbings, J. Phys. B **33**, 3225 (2000).
[61] H. Knudsen and J. F. Reading, Phys. Rep. **212**, 107 (1992).
[62] J. H. McGuire, N. Berrah, R. J. Bertlett, J. A. R. Samson, J. A. Tanis, C. L. Cocke, and A. S. Schlachter, J. Phys. B **28**, 913 (1995).
[63] G. Handke, F. Tarantelli, A. Sgamellotti, and L. S. Cederbaum, J. Electron Spectrosc. Relat. Phenom. **76**, 307 (1995).
[64] G. Handke, F. Tarantelli, and L. S. Cederbaum, Phys. Rev. Lett. **76**, 896 (1996).
[65] G. Handke, F. Tarantelli, and A. Sgamellotti, J. Chem. Phys. **104**, 9531 (1996).
[66] In representing the electron impact data of Tian and Vidal, we have taken the total cross section for triple ionization of CO by 100 eV electrons to be 1.14×10^{-19} cm^2 instead of the value listed in Table III of Ref. [22].
[67] I. Ben-Itzhak, T. J. Gray, J. C. Legg, and J. H. McGuire, Phys. Rev. A **37**, 3685 (1988).
[68] V. Krishnamurthi, K. Nagesha, V. R. Marathe, and D. Mathur, Phys. Rev. A **44**, 5460 (1991).
[69] G. Dawber, A. G. McConkey, L. Avald, M. A. MacDonald, G. C. King, and R. I. Hall, J. Phys. B **27**, 2191 (1994).
[70] M. Hochlaf, R. I. Hall, F. Penent, H. Kjedsen, P. Lablanquie, M. Lavollee, and J. H. D. Eland, Chem. Phys. **207**, 159 (1996).
[71] M. Lundqvist, P. Baltzer, D. Edvardsson, L. Karlsson, and B. Wannberg, Phys. Rev. Lett. **75**, 1058 (1995).
[72] F. Penent, R. I. Hall, R. Panajotovic, J. H. D. Eland, G. Chaplier, and Pl Lablanquie, Phys. Rev. Lett. **81**, 3619 (1998).
[73] J. P. Bouhnik, I. Gertner, B. Rosner, Z. Amitay, O. Heber, D. Zajfman, E. Y. Sidky, and I. Ben-Itzhak, Phys. Rev. A **63**, 032509 (2001).
[74] N. Bohr and J. Lindhard, K. Dan. Vidensk. Selsk. Mat. Fys. Medd. **28**, (7) (1954).
[75] K. Okada and S. Iwato, J. Chem. Phys. **112**, 1804 (2000).